Proceedings of the 9th World Congress on Electrical Engineering and Computer Systems and Sciences (EECSS'23)
Brunel University, London, United Kingdom – August 03-05, 2023
Paper No. ICBES 127
DOI: 10.11159/icbes23.127

In-Vivo Animal Trial of a Fiber-Optic Pressure Sensor Probe with Distributed Sensing Points for the Diagnosis of Lumbar Spinal Stenosis

Marvin Friedemann[1], Susanne Barz[2], Sebastian Voigt[1], Thomas Barz[3], Markus Melloh[4], Axel Müller[1], Jan Mehner[1]
[1]Chemnitz University of Technology, Department of Electrical Engineering and Information Technology
Reichenhainer Straße 70, 09126 Chemnitz, Germany
marvin.friedemann@etit.tu-chemnitz.de
[2]University Medical Center Rostock
Rostock, Germany
susanne.barz@med.uni-rostock.de
[3]Orthopedic Practice Greifswald
Greifswald, Germany
[4]Victoria University of Wellington
Wellington, New Zealand

Abstract - This paper reports a fiber-optic pressure sensor probe with multiple measuring points for simultaneous time and location resolved pressure sensing. Two different measurement principles were combined to a hybrid sensor which allows sensing before, along and after stenosis at the same time. At the tip a Fabry-Pérot-Interferometer is formed by a reflective multilayer membrane of a pressure sensor chip and an optical fiber. The sealed cavity provides absolute pressure sensing. 20 millimeter below the fiber tip, six Fiber Bragg Gratings are integrated. The first Fiber Bragg Grating is reinforced for additional temperature sensing. The five following Fiber Bragg Gratings act as sensing array for continuous pressure monitoring. The sensing components are coated with a silicone mantle of 1.5 mm diameter. The complete signal evaluation is done with a Fiber Bragg Grating interrogation device. The in-vivo trial with a pig allowed the determination of pressure relations and pulse wave velocity in the lumbar spinal canal. A stenosis was simulated by inflating a balloon inserted in parallel to the probe. For the first time, lumbar spinal stenosis was diagnosed by the measurement technique of the presented probe. This is a new diagnostic approach to verify the indication for surgery. First, mechanical structure aspects and the evaluation technique of our probe is described. Then, experimental results of the in-vivo trial are presented. From these results the possibility of implementing a new diagnostic method for the frequent lumbar spinal stenosis disease with claudication using to our sensing system could be derived.

Keywords**:** Fiber-optic sensors, Fabry-Pérot-Interferometer, Fiber Bragg Grating, distributed pressure sensor, sensor array, Lumbar spinal stenosis, in-vivo animal trial

1. Introduction

The invasive monitoring of vital parameters like pressure or temperature has a huge significance for diagnosis of hollow organs or vessels. Fiber-optic sensors offer a broad range of advantages. Their signal linearity, small size, and electromagnetic compatibility due to the non-electric sensing principles make fiber-optic sensors attractive for medical applications [1-3]. Especially the multiplexing ability takes effect when combining multiple measuring points into a single probe. Among them, a Fiber Bragg Grating (FBG) and a Fabry-Pérot-Interferometer (FPI) are predestined for the implementation of a sensor combination. Poeggel et al. and Duraibabu et al. introduced a fiber-optic sensor system for the application in urodynamics based on an extrinsic FPI and an FBG [4-6]. Arkwright et al. developed a manometry catheter based on multiple FBGs for measurement and diagnosis of the peristalsis in the human gut [7-9]. Potential applications for fiber-optic sensors could be examinations and diagnosis of lumbar spinal stenosis (LSS) or blood pressure measurement. LSS, the narrowing of the spinal canal with a compression of the epidural sac and nerve roots, associated with pain, claudication, and immobility is one of the most common spinal disorders in the elderly [10]. Surgical treatment for LSS is

one of the most frequent spinal interventions [11-13]. Increased epidural pressure at the level of stenosis has been identified as a reason for clinical symptoms but this parameter has not been established yet, since the measurement by invasive single-point sensors has not been feasible [14].

This paper introduces a hybrid pressure sensor probe based on a Fiber Tip Fabry-Pérot-Interferometer (FTFPI) and an FBG array for in-vivo examinations on LSS. The sensing structure comprises a microelectromechanical system pressure sensor chip with 600 µm diameter at the tip of a 125 µm optical silicate glass fiber with six FBGs. The front pressure sensor is formed by the reflective multilayer membrane of the chip realizing the interferometer principle for measuring absolute pressure. 20 mm after the tip, a reinforced FBG provides temperature sensing for potential compensation. The following five distributed pressure sensors with a pitch of 8 mm along the probe ensure time and space resolution of pressure measurement. The probe has an outer diameter of 1.5 mm, covered with medical silicone. The hybrid sensor is read out by a stabilized FBG interrogation device using a broadband light source. The probe serves as the proof of principle for the application as a new diagnosis tool for examinations on LSS. An approved in-vivo animal trial with a pig provides the experimental setup. Pressure variations depending on heartbeats and respiration were separated via curve fitting and calculated with shifts of the evaluated sensor wavelengths. The wave velocity through the spinal canal was determined with peak find algorithms for the time delay of the pulse wave maxima per distributed sensor.

2. Medical Background

The epidural pressure is a result of complex cerebral and spinal processes modulated by blood pressure, respiration and posture in relation to the dimensions of the spinal canal and the dural sac leading to a craniocaudal superposed pulse wave. We hypothesized that the normal epidural pulse wave is modified at the level of a relevant LSS. So far, there is no report on a dedicated sensor system for distributed pressure and pulse wave velocity measurement in the spinal canal. The use of our new sensor system with simultaneous pressure measurement at different points along the spinal canal makes it possible to identify patients who would benefit from surgery and avoid unnecessary interventions.

Simultaneous measurement of all sensing points before, along and after the LSS provides diagnosis of LSS and its location. During the approved animal experiment with a 50 kg pig, the introduced hybrid sensor probe was inserted into the spinal canal under X-ray control after laminectomy. With this surgical procedure the posterior bony roof of spinal canal was removed in one level of lumbar spine. Following this and basic measurements, a balloon was inserted. The subsequent inflating of the balloon simulated the presence of LSS. Fig. 1 shows anatomical conditions of the experimental approach and X-ray of the inserted probe.

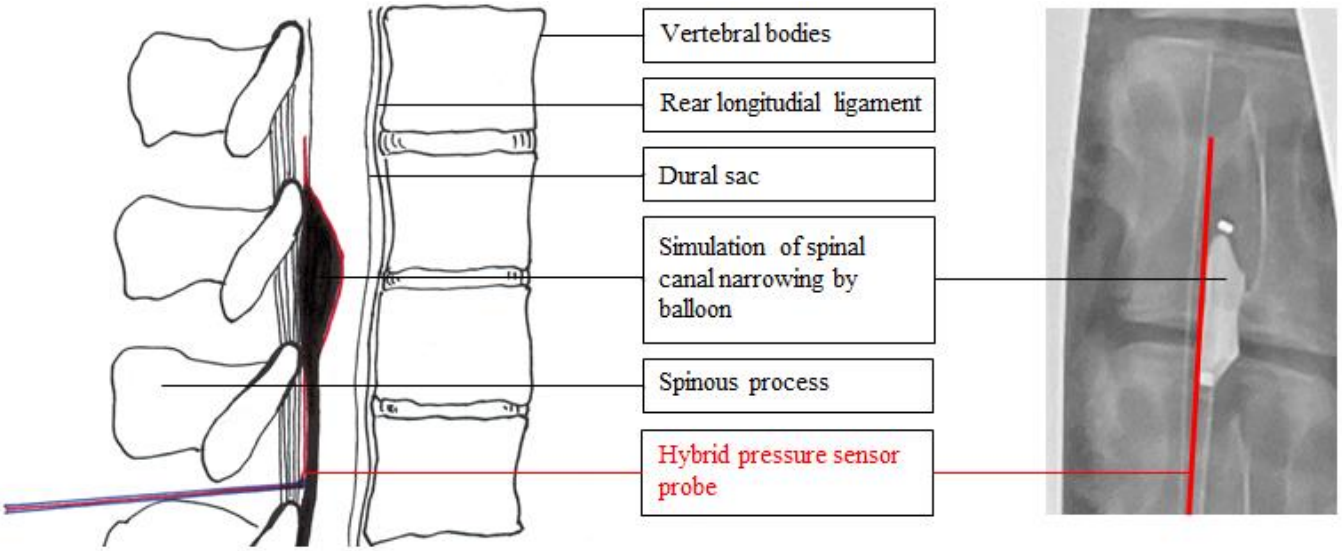

Fig. 1: Anatomy of the spinal column with simulated LSS under X-ray and sensor probe next to the balloon.

3. Hybrid Sensor Design

3.1. Pressure Sensor Chip

The pressure sensor chip is circular shaped, has an outer diameter of 600 µm and a total height of about 400 µm. The The multilayer membrane has a diameter of 200 µm and consists of 1 µm silicon dioxide (SiO_2), 100 nm platinum (Pt) and 600 nm aluminum nitride (AlN). Aluminum (Al) forms the top electrodes (see Figure 2) [15]. A 200 µm hole on the backside enables the insertion and central placement of the optical fiber. Due to the piezoelectric properties of the AlN layer the pressure sensor chip can be operated in a closed loop mode [16]. In this contribution we will use it as a passive membrane. With the passive principle, a smaller probe diameter is possible as electrical connection is space consuming.

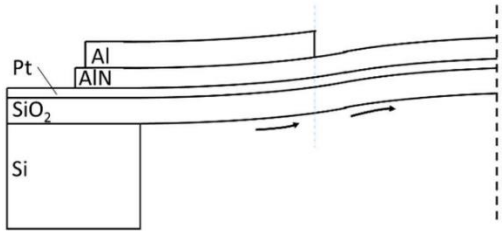

Fig. 2: Schematic cross section of the multilayer membrane [15].

3.2. Fiber Tip Fabry-Pérot-Interferometer

An FPI is a phase-modulated optical measuring instrument, typically consisting of two reflective planes. The space between both planes is called cavity. The cavity is formed between the reflective membrane and the fiber tip. Induced light produces interference due to the superposition of the light waves as a consequence of optical path difference (OPD). The OPD describes the length of the cavity. The shape of the interference pattern varies depending on the value of the OPD [17]. We observe that changes in hydrostatic pressure and ambient temperature result in shifts of the wavelength peaks in the interference pattern. The mean value of the peak shifts from the most intense maximums is tracked as measure for hydrostatic pressure changes and for calibration of the pressure sensor. Due to the sealed cavity, the FTFPI constitutes the absolute pressure sensing element of the probe. The evaluation principle is specified in [18]. Other possibilities of the interference pattern signal evaluation are Fringe Counting or Fourier-Transformation [19].

3.3. Fiber Bragg Gratings

An FBG is a periodic change within the respective refractive index of the optical fiber core from a mean value n_{eff} above a length with the grating periodicity Λ. Light wave interferences between these grating planes result in reflections of a wavelength peak, the Bragg wavelength λ_B. The residual spectrum is unaffected. Longitudinal expansion and thermal exposure of the FBG result in a change of the Bragg wavelength. A rising ambient temperature implicates an increase of n_{eff}, induced by the thermo-optic effect and thermal expansion. Strain raises the distance of grating planes Λ and also increases n_{eff} due to the photoelastic effect [3, 20]. A sensor array is generated due to the multiplexing ability of FBGs. When inscribing FBGs with different grating planes in a single optical fiber, different Bragg wavelength were reflected and evaluated simultaneously. By covering the optical fiber with a polymer, it is possible to convert pressure impacts to corresponding linear shifts of the Bragg wavelength. This is the applied principle for time and location distributed pressure sensing. The FBG array identifies relative pressure variations relating to the absolute pressure at fiber tip.

3.4. Mechanical Structure of the Probe

The assembly procedure of the pressure sensor probe is a lab based manual approach as we report this paper. The optical fiber is placed orthogonal to the pressure sensor chip membrane using x-y-z manipulators of a wafer probe station, while controlling the interference pattern to prevent membrane damage through harsh contact with the fiber tip. Adhesive ensures a fixation at a stable position and a sealing of the cavity around the fiber in front of the tip for pressure sensing. Then, the optical fiber gets coated above the length of the first FBG by a thin adhesive film for reinforcement. With this measure the sensitivity of this FBG against strain respectively pressure was strongly reduced to use it as almost temperature only sensing

element. The temperature compensating strategy was introduced in [21]. The sensitive area consisting of FTFPI, coated temperature FBG (FBG_T) and five pressure sensing FBGs is sealed with medical silicone to reach an outer diameter of 1.5 mm. A guidewire added during potting ensures an increased stiffness of the probe for surgical handling. Below the sensitive area, a protection cover forms the handpiece of the probe. Fig. 3 demonstrates the schematic structure of the sensitive probe tip and Fig. 4 shows photograph of the probe just before surgical insertion.

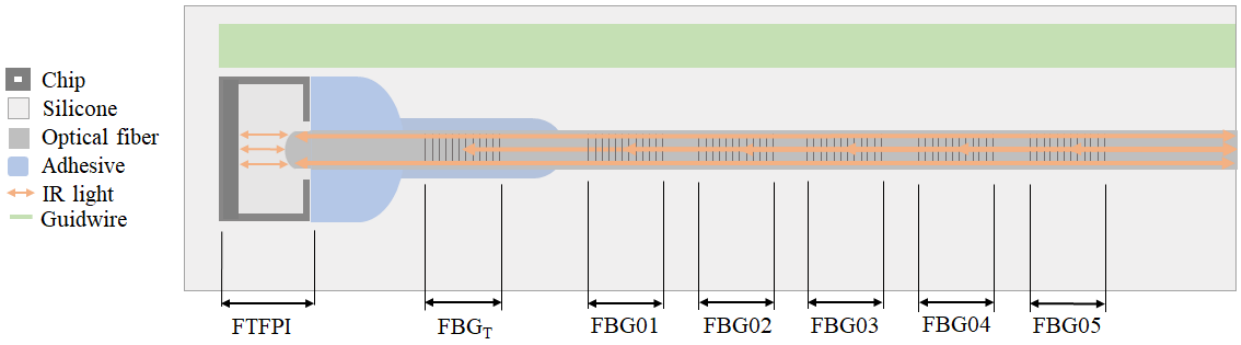

Fig. 3: Schematic cross section of the sensitive area.

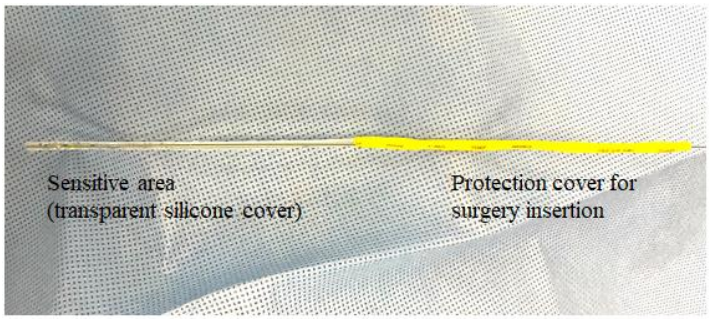

Fig. 4: Photograph of the inserted probe.

3.5. Signal processing

The readout device comprises a superluminescent diode (SLED), a spectrometer (including optical components and an image sensor) and is designed to be used to interrogate FBGs. Broadband light is coupled into the optical fiber. The SLED includes a circulator for transmitting the superposed FTFPI and FBG signal (see Fig. 5) to the spectrometer. The tracking and readout of different peak shifts are done by a LabView based software. The signal processing setup is essential for simultaneous evaluation of all sensing points. Thus, the estimation of time and spatially resolved pressure distribution is possible. The opto-electronical components are stabilized by controlled heating to a constant temperature for drift prevention [22].

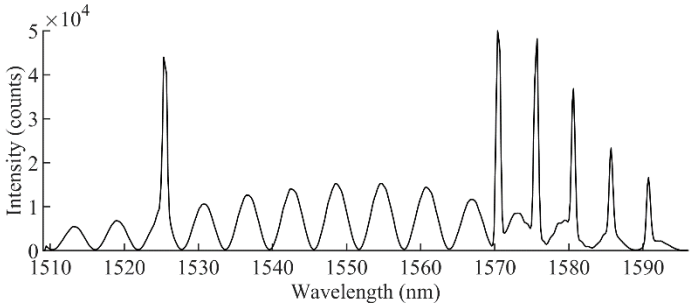

Fig. 5: Optical spectrum of superposed FTFPI and FBG signals.

4. In-Vivo Animal Trial

4.1. Measurement Preparation

For calibration of the sensing points the probe was inserted into a vascular model. The previously developed vascular vascular model is based on an electrical pump, compressed air system, polymer hoses, reference sensors and water [23]. A water column and the compressed air system generates various hydrostatic pressure values. This will be used for evaluation of the pressure sensitivity of the FTFPI and the FBGs. The temperature dependence of the probe is determined by controlled heating of the surrounding water, which is important for calibration options.

The calibration process revealed a pressure sensitivity of about -5 pm/mmHg for the FTFPI. The sensitivity of the five distributed pressure sensing FBGs is approximately 0.75 pm/mmHg. The reinforced temperature compensating FBG_T has an insignificant low pressure sensitivity which is not measurable. Due to different evaluation algorithms of FTFPI and FBG and thus different resolutions (FBG evaluation resolution ≈ 0.5 pm, FTFPI evaluation resolution ≈ 2 pm) both sensitivities are in the same range. The temperature dependence is about 0.3 nm/K for the FTFPI, 0.018 nm/K for the FBG_T and 0.024 nm/K for the pressure sensing FBGs.

4.2. Medical Setup

During the complete procedure (Fig. 6) the pig was under general anaesthesia and intubated for machine ventilation. An applied medical monitoring which included i. a. electrocardiogram, blood pressure, respiratory rate and body temperature ensures stable conditions and comparative values. Because of an almost constant body temperature of 37.4 °C during the whole experiment, a temperature compensation was not necessary as calibration is applicable at the same conditions.

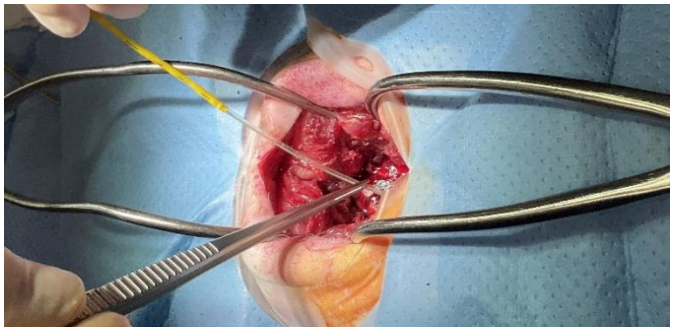

Fig. 6: Surgical insertion of the probe at the in-vivo trial.

4.3. Epidural pressure and heart rate

The FTFPI provides the value for the obtaining pressure level in the lumbar spinal canal. Fig. 7 shows the absolute pressure in the lumbar spinal canal of approximately 7.5 mmHg without balloon catheter and stenosis. The pulse waves generated by the pulmonary and cardiovascular system are also measurable in the spinal canal. Their peak-to-peak value is almost 4 mmHg. The heart rate is about 84 min^{-1}. The pulse waves are generated due to the pulsatile liquor inside the spinal canal which is coupled to the cardiovascular system [24-26].

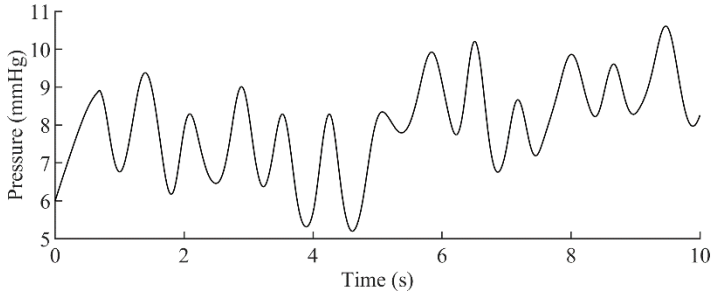

Fig. 7: Range of epidural pressure and pulse waves in lumbar spinal canal without simulated LSS.

4.4. Pulse wave velocity

When analysing the pressure values measured by the FBG array the heart rate (≈ 84 min^{-1}) as well as the breath rate (≈ 18 min^{-1}) is determinable. The time and location resolved relative pressure distribution along the FBG array within a breath is plotted in Fig. 8. The time lag between the heart beat induced pulse maximums on each FBG presents the movement of the pressure wave along the probe. By means of a maxima detection algorithm every pulse wave maximum on each FBG is determined (marked with "+" on the diagram). The pulse wave time lag between the FBGs is reproducible in each heart beat. An average pulse wave velocity of about 0.97 m/s is calculated applying the time lag of the pulse wave maximums between the FBGs to the distance between FBG01 and FBG05. The increasing offset is the respiration induced pressure variation of approximately 12 mmHg peak-to-peak per breath.

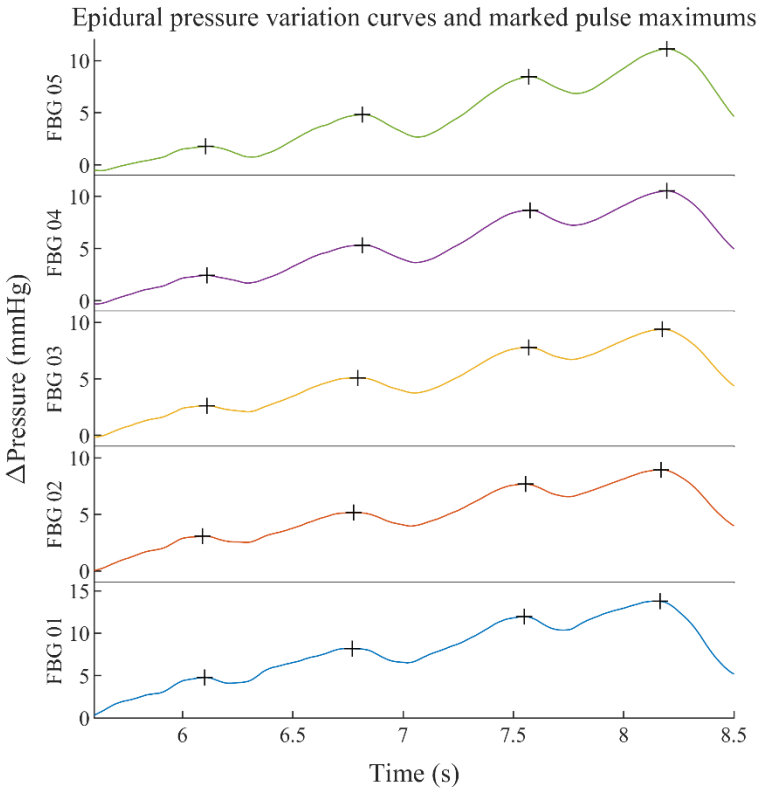

Fig. 8: Movement of the pulse waves within the spinal canal along the FBG array.

4.5. Stenosis localisation diagnosis

After measuring the normal epidural pressure relations in the lumbar spinal canal the balloon was inflated successively until its highest expansion. Simultaneous measurement along all sensing points gives an overview about stenosis manifestation in real time. The wavelength data is plotted in Fig. 9. The propagation of the pulse waves stops after FBG01. The lower frequency still detectable by all FBGs are equal to the respiration rate. In the following sensing points (FBG02-FBG05) no coherent pulse waves are detectable. The high amplitude shift in the curve of FBG01 is due to bending and compression of the probe. The large expansion of the balloon generates strong mechanical impact on the spinal canal anatomy as well as the sensor probe. Therefore, measured pressure values are affected by mechanics and the scale is not converted to mmHg (e.g. peak-to-peak value of pulse waves at FBG01 is more than three times higher than without inflated balloon). Nevertheless, the pulse waves and the difference at stenosis are clearly determinable and a decisive parameter for stenosis localisation is measurable unbiased by amplitude. Coherent pulse waves corresponding to the heart beat are no longer detectable distal to FBG01. Consequently, the stenosis is located directly distal FBG01.

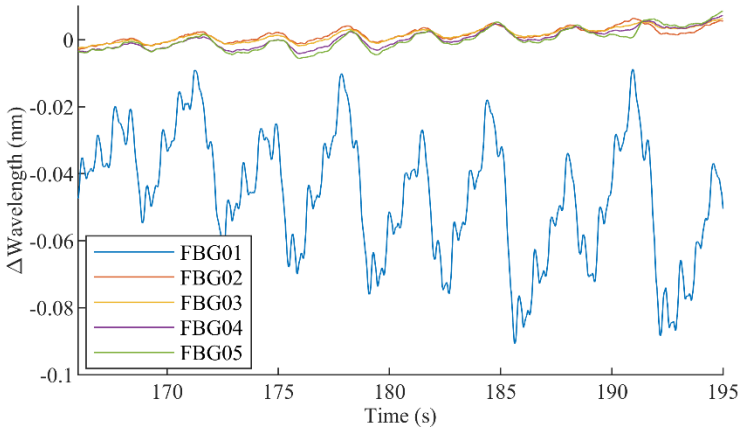

Fig. 9: Demonstration of the relation between narrowing location (FBG01) and no longer detectable pulse waves distal of the stenosis (FBG02 to FBG05).

5. Conclusion

With the introduced fiber-optic pressure sensor probe a completely new possibility for investigations on lumbar spinal stenosis is presented. Simultaneously evaluation of multiple measurement points provides the time and location resolved sensing of pressure distribution in real time. The calibration of the hybrid sensor system revealed a sensitivity of -5 pm/mmHg for the fiber-tip pressure sensor and 0.75 pm/mmHg for the distributed sensors. The pulse wave through the spinal canal without stenosis has a peak-to-peak value of about 4 mmHg, averaged over multiple amplitudes. Breaths superpose the pressure curve with about 12 mmHg. A pulse wave velocity of about 0.97 m/s was determined. The simulated LSS was detected in real time due to no longer detectable pulse waves distal of the stenosis and a huge amplitude at the first of five distributed pressure sensors along the narrowing. These results confirm our hypothesis that normal epidural pulse wave is modified at the level of a relevant LSS. Our pressure sensor system provides a new reliable and safe method for detection, location and grading of central LSS.

Acknowledgements

Both authors contributed equally to this paper.

References

[1] D. Tosi, S. Poeggel, I. Iordachita, and E. Schena, “Fiber Optic Sensors for Biomedical Applications”, in *Opto-Mechanical Fiber Optic Sensors*: Elsevier, 2018, pp. 301–333.

[2] P. Roriz, O. Frazão, A. B. Lobo-Ribeiro, J. L. Santos, and J. A. Simões, “Review of fiber-optic pressure sensors for biomedical and biomechanical applications”, *Journal of Biomedical Optics*, vol. 18, no. 5, pp. 50903-1–50903-18, 2013.

[3] A. Othonos and K. Kalli, *Fiber Bragg gratings: Fundamentals and applications in telecommunications and sensing*. Boston, Mass.: Artech House, 1999.

[4] D. Duraibabu, N. Kelly, S. Poeggel, H. Flood, H. Yuan, G. Dooly, D. McGrath, D. Tosi, E. Lewis, and G. Leen, “Optical fibre pressure and temperature sensor system designed for urodynamic applications”, in *SPIE Proceedings*, 2016.

[5] S. Poeggel, D. Duraibabu, D. Tosi, G. Leen, E. Lewis, D. McGrath, F. Fusco, S. Sannino, L. Lupoli, J. Ippolito, and V. Mirone, “Differential in vivo urodynamic measurement in a single thin catheter based on two optical fiber pressure sensors”, *Journal of Biomedical Optics*, vol. 20, no. 3, pp. 37005-1–37005-9, 2015.

[6] S. Poeggel, D. Tosi, F. Fusco, J. Ippolito, L. Lupoli, V. Mirone, S. Sannino, G. Leen, and E. Lewis, “Fiber-Optic EFPI Pressure Sensors for In Vivo Urodynamic Analysis”, *IEEE Sensors Journal*, vol. 14, no. 7, pp. 2335–2340, 2014.

[7] J. W. Arkwright and I. Underhill, “Fibre Bragg grating manometry catheters for in vivo monitoring of peristalsis”, in *Advanced Biomedical and Clinical Diagnostic and Surgical Guidance Systems XV*, 2017.

[8] J. W. Arkwright, N. G. Blenman, I. D. Underhill, S. A. Maunder, N. J. Spencer, M. Costa, S. J. Brookes, M. M. Szczesniak, and P. G. Dinning, "Measurement of Muscular Activity Associated With Peristalsis in the Human Gut Using Fiber Bragg Grating Arrays", *IEEE Sensors Journal*, vol. 12, no. 1, pp. 113–117, 2012.
[9] J. W. Arkwright, N. G. Blenman, I. D. Underhill, S. A. Maunder, M. M. Szczesniak, P. G. Dinning, and I. J. Cook, "In-vivo demonstration of a high resolution optical fiber manometry catheter for diagnosis of gastrointestinal motility disorders", *Optics Express*, vol. 17, no. 6, pp. 4500–4508, 2009.
[10] T. Deer, D. Sayed, J. Michels, Y. Josephson, S. Li, and A. K. Calodney, "A Review of Lumbar Spinal Stenosis with Intermittent Neurogenic Claudication: Disease and Diagnosis", *Pain Medicine*, vol. 20, Supplement_2, S32-S44, 2019.
[11] C. Bagley, M. MacAllister, L. Dosselman, J. Moreno, S. G. Aoun, and T. Y. El Ahmadieh, "Current concepts and recent advances in understanding and managing lumbar spine stenosis", *F1000Research*, vol. 8, 2019.
[12] M. V. Boswell, A. M. Trescot, S. Datta, D. M. Schultz, H. C. Hansen, S. Abdi, N. Sehgal, R. V. Shah, V. Singh, R. M. Benyamin, V. B. Patel, R. M. Buenaventura, J. D. Colson, H. J. Cordner, R. S. Epter, J. F. Jasper, E. E. Dunbar, S. L. Atluri, R. C. Bowman, T. R. Deer, J. R. Swicegood, P. S. Staats, H. S. Smith, A. W. Burton, D. S. Kloth, J. Giordano, and L. Manchikanti, "Interventional techniques: evidence-based practice guidelines in the management of chronic spinal pain", *Pain physician*, vol. 10, no. 1, pp. 7–111, 2007.
[13] T. Amundsen, H. Weber, H. J. Nordal, B. Magnaes, M. Abdelnoor, and F. Lilleâs, "Lumbar spinal stenosis: conservative or surgical management?: A prospective 10-year study", *Spine*, vol. 25, no. 11, 1424-35; discussion 1435-6, 2000.
[14] T. Barz, M. Melloh, L. P. Staub, S. J. Lord, J. Lange, and H. R. Merk, "Increased intraoperative epidural pressure in lumbar spinal stenosis patients with a positive nerve root sedimentation sign", *European Spine Journal*, vol. 23, no. 5, pp. 985–990, 2013.
[15] C. Stoeckel, K. Meinel, M. Melzer, and T. Otto, "Thin Film Piezoelectric Aluminum Nitride for Piezoelectric Micromachined Ultrasonic Transducers", in *2018 IEEE SENSORS*, New Delhi, India, 2018, pp. 1–4.
[16] M. Friedemann, S. Voigt, D. Kriebel, K. Meinel, C. Stoeckel, R. Hecker, K. Hiller, and J. Mehner, "Pressure Sensor Catheter based on piezoelectric actuated Aluminum Nitride Membrane and Fiber Tip Fabry-Perot-Interferometer", in *MikroSystemTechnik Congress 2021; Congress*, 2021, pp. 155–158.
[17] S. Tofighi, A. Bahrampour, N. Pishbin, and A. R. Bahrampour, "Interferometric Fiber-Optic Sensors", in *Optical Fiber Sensors: Advanced Techniques and Applications*, G. Rajan and K. Iniewski, Ed. Boca Raton, FL: CRC Press, 2015, pp. 37–78.
[18] M. Friedemann, S. Voigt, D. Kriebel, C. Stoeckel, K. Meinel, R. Hecker, K. Hiller, and J. Mehner, "Pressure Sensor Catheter based on Micromachined Aluminum Nitride Membrane Fiber Tip Fabry-Pérot-Interferometer", in *2021 International Conference on Applied Electronics (AE)*, 2021.
[19] Y.-J. Rao, Z.-L. Ran, and Y. Gong, "Interrogation and Multiplexing Techniques for FFP Sensors", in *Fiber-Optic Fabry-Perot Sensors: An Introduction*. Boca Raton, London, New York: CRC Press Taylor & Francis Group, 2017, pp. 129–153.
[20] M. M. Werneck, R. C. S. B. Allil, B. A. Ribeiro, and F. V. B. de Nazaré, "A Guide to Fiber Bragg Grating Sensors", in *Current Trends in Short- and Long-period Fiber Gratings*, C. Cuadrado-Laborde, Ed.: InTech, 2013.
[21] M. Friedemann, S. Voigt, and J. Mehner, "Pressure sensor catheter based on Fiber Tip Fabry-Pérot-Interferometer and Fiber Bragg Grating for temperature compensation", *Current Directions in Biomedical Engineering*, vol. 8, no. 2, pp. 404–407, 2022.
[22] M. Friedemann, S. Voigt, M.-L. Werner, R. Hecker, and J. Mehner, "Drift analysis and stabilization of a Fiber Bragg Grating interrogation device", in *2020 International Conference on Applied Electronics (AE)*, 2020.
[23] M. Friedemann, S. Voigt, R. Otto, and J. Mehner, "In-Vitro Verifikation medizinischer Drucksensoren am dynamischen Gefäßmodell", in *15. Chemnitzer Fachtagung Mikromechanik & Mikroelektronik*, 2022, pp. 134–138.
[24] T. Brinker, E. Stopa, J. Morrison, and P. Klinge, "A new look at cerebrospinal fluid circulation", *Fluids and Barriers of the CNS*, vol. 11, no. 1, 2014.
[25] L. Sakka, G. Coll, and J. Chazal, "Anatomy and physiology of cerebrospinal fluid", *European Annals of Otorhinolaryngology, Head and Neck Diseases*, vol. 128, no. 6, pp. 309–316, 2011.

[26] B. Sweetman and A. A. Linninger, “Cerebrospinal Fluid Flow Dynamics in the Central Nervous System”, *Annals of Biomedical Engineering*, vol. 39, no. 1, pp. 484–496, 2010.